

Chiral and directional optical emission from a dipole source coupled to a helical plasmonic antenna

Lilli Kuen,^{1,2} Lorenz Löffler,³ Aleksei Tsarapkin,⁴ Lin Zschiedrich,² Thorsten Feichtner,³ Sven Burger,^{1,2} and Katja Höflich⁴

¹⁾Zuse Institute Berlin, Takustraße 7, 14195 Berlin, Germany

²⁾JCMwave GmbH, Bolivarallee 22, 14050 Berlin, Germany

³⁾Experimental Physics 5, Institute of Physics, University of Würzburg, Germany

⁴⁾Ferdinand-Braun-Institut, Leibniz-Institut für Höchstfrequenztechnik, 12489 Berlin, Germany

Plasmonic antennas with helical geometry are capable transducers between linearly polarized dipole emission and purely circular polarized far-fields. Besides large Purcell enhancements they possess a wide tunability due to the geometry dependence of their resonant modes. Here, the coupling of a dipole emitter embedded in a thin film to plasmonic single and double helices is numerically studied. Using a higher-order finite element method (FEM) the wavelength dependent Purcell enhancement of a dipole with different positions and orientations is calculated and the far-fields with respect to their chirality and radiation patterns are analyzed. Both single and double helices demonstrate highly directional and circularly polarized far-fields for resonant excitation but with significantly improved directional radiation for the case of double helices.

Polarization is an important basic property of light related to the spin degree of freedom of its fundamental quanta, the photons. Right and left circularly polarized light corresponds to photons with spin $+1$ and -1 , respectively. Accordingly, controlling the degree of (circular) polarization allows the realization of different photonic quantum information protocols¹. Such protocols rely on the interference of single indistinguishable photons emitted by one or several non-classical light sources, so-called quantum emitters. While numerous advanced but macroscopic devices exist for photon polarization control, efficient implementation in future devices requires a nanoscale solution that combines strong light-matter interaction with a handle for setting or determining the polarization state².

In this regard, metallic nanostructures are advantageous since their free-electron gas can be excited into collective movement by incident light. The associated quasi-particle describing light coupled to electron density oscillations is named plasmon-polariton and features electromagnetic near-fields at the metal surface. Accordingly, the resonant excitation of a well-designed plasmonic antenna can exhibit confinement of optical fields several orders below the diffraction limit leading to extreme near-field concentration³. Therefore, plasmonic antennas provide an increased number of radiative decay channels for any dipolar emitter located in these fields leading to a correspondingly increased rate of spontaneous emission. This is captured in Purcell's formula⁴: $F = 3/(4\pi^2)(\lambda/n_m)^3 Q/V$, by the small mode volume. Here, F denotes the fluorophore's emission enhancement factor at a vacuum wavelength λ when placed in a resonators field maximum with quality factor Q and mode volume $V/(\lambda/n_m)^3$, where the emitter resides in a medium of refractive index n_m . This strongly enhanced light-matter interaction has already been used for sensing down to the single-molecule level e.g. in Raman scattering⁵ or molecular fluorescence^{6,7}.

Since plasmonic resonances are comparably broad and the internal quantum efficiency of the coupled emitter can approach unity, plasmonic antennas provide an exciting playground for all types of quantum emitters and their application as super-bright single photon sources⁸⁻¹⁰. Plasmonic antennas

on the other hand can be also designed to couple to specific radiating modes¹¹, and, therefore, e.g. achieve directional emission of quantum emitters of different types^{12,13} which is one of the main requirements for possible on-chip integration in a photonic architecture².

Helical plasmonic geometries enable strong chiroptical interaction. Arrays of helices were demonstrated to be transparent to one handedness of the incident light but reflective for the other¹⁴. Similarly strong responses were shown for single helices made from silver¹⁵ approaching the theoretical maximum of chiroptical interaction^{16,17}. Hence, combining a helical plasmonic antenna with a (dipolar) quantum emitter would be an exciting opportunity to control the state of polarization at the nanoscale, i.e. control the spin degree of freedom for single photons on a chip. First encouraging experimental results were achieved by creating a small slit at the bottom of a helical antenna mimicking a dipolar excitation source¹⁸.

Here, we numerically study the coupling of a linearly polarized dipolar emitter to two types of chiral plasmonic antennas: a single helix and a double helix. The emitter resides in a hexagonal Boron nitride (hBN) layer, with hBN being one of the prime emerging platforms for bright and stable quantum emitters¹⁹. For the single helix, a semi-analytical model is used to assess resonance positions and far-field patterns. The FEM modeling then treats the full scenarios of a linearly polarized dipole coupled to the helices to compute Purcell factors and detailed far-field emission characteristics. Efficient coupling of excited dipoles can be achieved for both helix types leading to circularly polarized directional emission along the helix axis.

Theoretical Background and Implementation – We investigate chiral plasmonic resonators made from silver²⁰ similarly to¹⁵ in the near-infrared regime arranged as single or double helices on a substrate (see Fig. 1). The single helix is defined by its radius $r_h = 60\text{nm}$, pitch height $h_p = 310\text{nm}$, amount of pitches p and wire radius $r_t = 32\text{nm}$, with right-handed orientation as depicted in Fig. 1(a). The double helix with four pitches combines two of these single helices, one rotated by 180 degrees along the helix axis, see Fig. 1(b). The substrate consists of 20 nm hBN²¹ on 20 nm Glass (BK7)²².

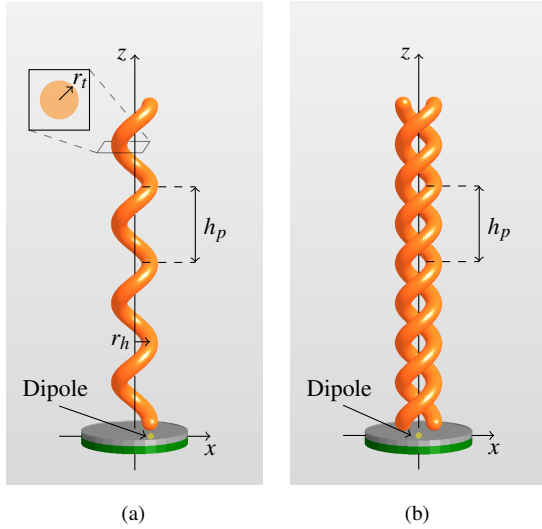


FIG. 1. Sketch of a single (a) and double (b) plasmonic helices with dipole emitter, pitch height h_p , helix radius r_h and tube radius r_t .

The helix ends dip 2 nm into the hBN in order to realize a finite contact area between metal and substrate, and to obtain smooth meshing. The entire setup is analyzed using a higher-order finite element method (FEM), implemented in the solver JCMsuite²³. The excitation is realized by a point source, described by a current density $\mathbf{J}(\mathbf{r}, t)$. For $\mathbf{r} \rightarrow \mathbf{r}_0$ with the position vector \mathbf{r} and the position of the point emitter \mathbf{r}_0 , the electric field diverges, which may affect the convergence of numerical results towards the exact solution. This problem is solved by a subtraction approach²⁴. The Purcell enhancement is computed as the ratio between the dipole emission in the full system compared to emission in bulk hBN. This provides information about how much dipole power is coupled to the adjacent structures. Due to the strong near-fields of resonant plasmonic structures, the radiative decay rate enhancement of dipolar emitters is extremely position-sensitive. In addition, if the emitter comes too close, quenching will occur^{25,26}. Hence, careful modelling of dipole position, geometries and materials is required.

With the vectorial three-dimensional field solution of the scattering simulation, the far-field can be calculated via Fourier transformation (cf. Supporting Information for more details). The degree of circular polarization in the far-field is retrieved to identify helix geometries able to transform linearly polarized dipole emission into circularly polarized light. Let w_{RCP} and w_{LCP} represent the amplitudes of the right-circularly polarized (RCP) and left-circularly polarized (LCP) components in the far-field in a given direction (for details see Supporting Information). The degree of circular polarization G is then defined as:

$$G = \frac{w_{\text{LCP}} - w_{\text{RCP}}}{w_{\text{LCP}} + w_{\text{RCP}}}, \quad (1)$$

which indicates in the range $[-1, 1]$ the degree of circular polarization from fully RCP to fully LCP. Technologically relevant is a directive large intensity of the far-field together with a

high degree of polarization. This is represented by the electric chirality density χ_e , given as²⁷

$$\chi_e = \frac{1}{8} (\mathbf{D}^* \cdot (\nabla \times \mathbf{E}) + \mathbf{E} \cdot (\nabla \times \mathbf{D}^*)), \quad (2)$$

where negative values correspond to RCP and positive values to LCP light.

Numerical Investigation of a Single Helix – First, a semi-analytical extension of the design tool of Höflich *et al.*¹⁵ (SA-DT) is used. It approximates a single helix in vacuum by an one-dimensional linear rod resonator for calculation of the plasmonic Fabry-Perot modes dependent on the rod's radius, length and material²⁸. The overlap integral between a mode and a circularly polarized plane-wave excitation determines the total power that is transferred to the rod, when curved into the final helix geometry¹¹. The far-field radiation patterns of these modes can be assessed by varying the angle of incidence of the plane waves due to the reciprocity of Maxwell's equations²⁹ (cf. Supporting Information for more detail). Figure 2(a) shows far-field patterns acquired with the SA-DT at the resonance positions of the helix modes with orders $n = 3, 4$, and 5 where n equals the number of positions with vanishing surface charge, called nodes. For $n = 3$, nearly no emission occurs along the helix axis followed by a maximum for increasing emission angles, another minimum and a third maximum along the plane perpendicular to the helix. The $n = 4$ mode exhibits one node per helix pitch corresponding to stacking the fundamental mode of the single pitch helix³⁰. In this case, all charge density maxima align along the z -axis which defines therefore also the net dipole orientation. This results in the distinct dipole-like side emission observed in the far-field pattern. Such an emission may be of interest for array/grating applications where the interaction of the elements leads to emerging lattice resonances^{31,32}. However, here we strive for the contrary, high directivity in z -direction to increase photon yield for any receiver/coupler for on-chip integration. This is delivered by the $n = 5$ mode.

For gaining a more complete understanding, the system is studied using full wave simulations using FEM and introducing a dipole emitter as the excitation source. The power of a point emitter transferred to a resonator depends on the strength and overlap of the plasmonic resonator mode fields with the field of the emitter – both classically and quantum mechanically³³. We investigate different positions and polarizations (x , y and z direction) of the dipole source. The position is varied along the x -axis from $[0 \text{ nm}, 90 \text{ nm}]$ in 10 nm steps, see sketch in Fig. 1(a). In the z -direction, the position of the dipole is located in the center of the 20 nm hBN layer, $\Delta z = 8 \text{ nm}$ below the helix end cap. For each position and polarization, the Purcell enhancement is computed for the wavelength range $\lambda = [800 \text{ nm}, 1800 \text{ nm}]$ (see Supporting Information). The optimum coupling is achieved for a z -polarized dipole located exactly below the end cap of the helix at $x = 60 \text{ nm}$ when the dipole is closest to the surface of the helix end cap. The helix near-fields are strongest here and the dipole orientation matches the dominant near-field orientation normal to the metallic surface.

For the best coupling scenario, the Purcell enhancement F

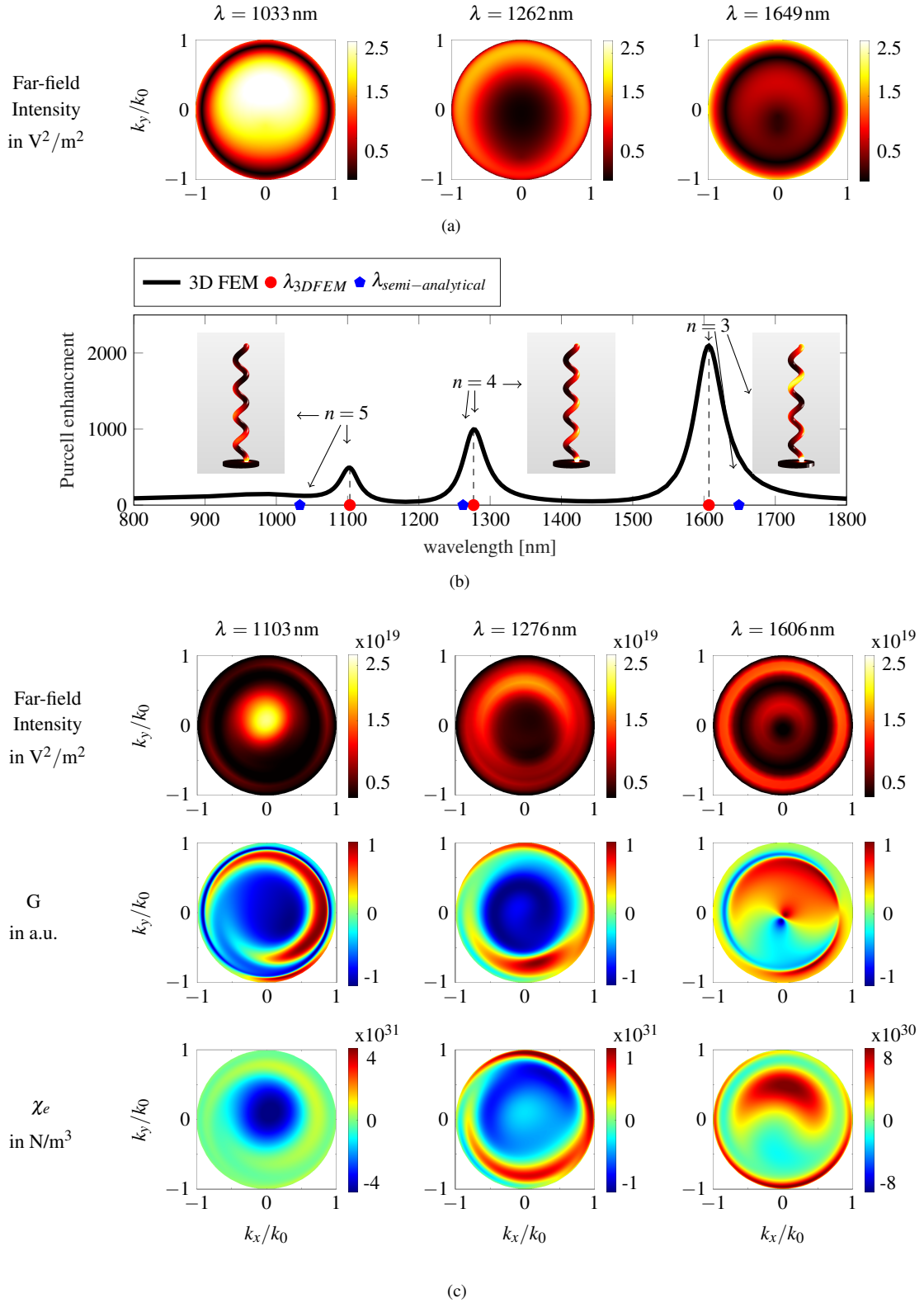


FIG. 2. Resonances and far-fields for the single helix with four pitches. (a) Far-field computed with the semi-analytical model. (b-c) Full 3D simulation results: (b) Purcell enhancement spectrum of a z -polarized dipole source at $x = 60$ nm, 8 nm below the helix end cap. Red (blue) dots indicate the resonance wavelengths from the full 3D (semi-analytical) results. Insets show visualisations of the induced field intensity on the helix surface at the resonance wavelengths. (c) Angular spectra of far field intensity, far-field degree of polarization G , and electric chirality density χ_e .

in dependence on the wavelength is shown in Fig. 2(b) together with the mode field patterns as insets. The graph displays three clear resonances at 1606nm, 1276nm and 1103nm with mode orders 3,4, and 5. For comparison, the mode positions obtained by SA-DT are denoted by blue pentagons. Lower order modes feature higher Purcell enhancement due to their smaller mode volume, while the quality factors Q are about 30 for all three resonances. This is comparable to the case of straight rod antennas³⁴.

Next, the far-field chirality properties G and χ_e are studied. The first row in Fig. 2(c) depicts far-field intensities obtained by the full-field model with dipole coupling for the three strong resonances. These closely resemble the results obtained from the semi-analytical approach but show an increased overall directivity, most probably caused by the influence of the substrate. The angle-dependent portions of LCP and RCP light in the far-field are shown in the second row of Fig. 2(c). For the $n = 3$ resonance at 1606nm, a critical point of helicity is directly along the helix axis. For the other two resonances at 1103nm and 1276nm, RCP light dominates for emission along the helix axis and LCP in the outer part for oblique emission. The electric chirality density χ_e is depicted in the third row of Fig. 2(c). This quantity provides a measure for the strength of chiroptical interaction which requires both field intensity and chirality. The resonances at 1103nm and 1276nm exhibit a negative χ_e in the center corresponding to high-intensity RCP light emission for small angles. However, the intensity distribution of the $n = 4$ resonance in the far-field is unfavorable for directional emission, as it decreases in the very center. In addition, χ_e shows large variations at higher angles making it hard to selectively address a specific handedness of light. The same holds true for the $n = 3$ resonance at 1606nm, where the far-field intensity corresponds to a higher order multipole emission and is therefore significantly weaker for emission along the antenna axis than for oblique emission. Thus, only the $n = 5$ resonance at 1103nm provides both, strongly directional emission of pure circularly polarized light. The price for this is the lower Purcell enhancement compared to the lower order modes. A possibility to achieve directional emission for these modes as well would therefore be highly desirable.

For this reason, we introduce in the following double helices that are C2 symmetric along the z -axis.

Numerical Investigation of Double Helices – Next, helices with the same geometrical parameters but in a double helix configuration and differing number of pitches p are studied. The excitation is realized by placing a dipole in the midpoint of the radius of the helix at the center of the hBN with its dipole moment oriented to point in the direction of both wires (here, x -axis), see Fig. 1(b). This in-plane alignment of the dipolar emitter is common for hBN color centers^{35,36}. The central position was chosen as compromise between excitation efficiency and quenching²⁶.

Fig. 3(a) displays the spectral dependency of the Purcell enhancement in the near-infrared range where one dominant resonance occurs at wavelengths of $\lambda = 1720$ nm for one, $\lambda = 1637$ nm for two, $\lambda = 1608$ nm for three, and $\lambda = 1595$ nm for four pitches. As can be seen in the surface intensity plots

below, this is the resonance with one dipole per helix pitch, equaling a mode order of $n = 1$ for one pitch up to mode order $n = 4$ for four pitches. The mode positions vary since the relative influence of the wire radius increases with decreasing wire length affecting the effective plasmon wavelength^{15,28}.

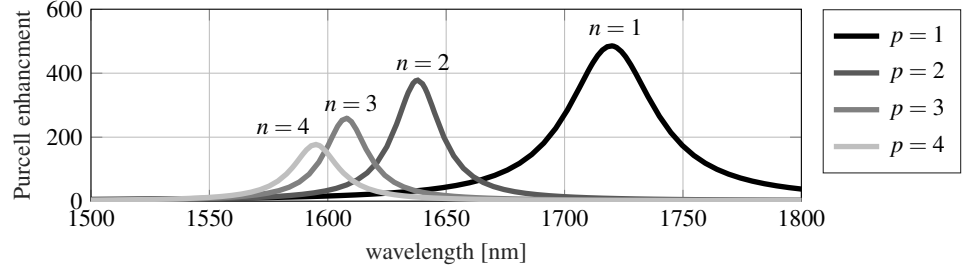
The strength of the Purcell enhancement decreases for increasing double helix pitches due to the increasing mode volume of the resonances. Note, that the absolute Purcell enhancement values cannot be compared to the single helix results as distance and orientation between emitter and the helices differ. The quality factor for the single pitch double helix is comparable to that of the single helix modes with $Q_{p=1} = 39$, while the double helices with 2, 3, and 4 pitches exhibit roughly doubled quality factors of $Q_{p=2} = 66$, $Q_{p=3} = 76$, and $Q_{p=4} = 66$.

Compared to the single helix geometry with 4 pitches where the $n = 4$ resonance was at $\lambda = 1276$ nm the near-field coupling between the helix arms causes a strong red-shift with the same mode order now appearing at $\lambda = 1595$ nm³⁷. This antisymmetric coupling leads to effective dipole moments in the x - y -plane that radiate mainly in z -direction and interfere according to their relative phase difference. A simple model that explains the emission strength based on phase differences of dipoles stacked along the z -axis can be found in the Supporting Information. Accordingly, the resulting net dipole moment has a high chance to be oriented in the x - y -plane leading to the desired strongly directional emission. The first row of Fig. 3(f) shows the far-field radiation patterns which indeed prove the directivity along the z -axis. Only in the case of $p = 3$ the highest intensity can be found in two side lobes and not within the center of the far-field due to destructive interference (cf. Supporting Information for more details).

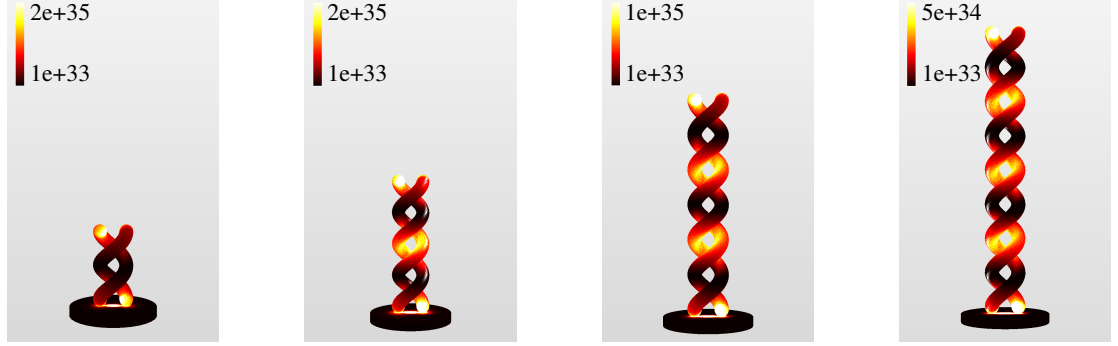
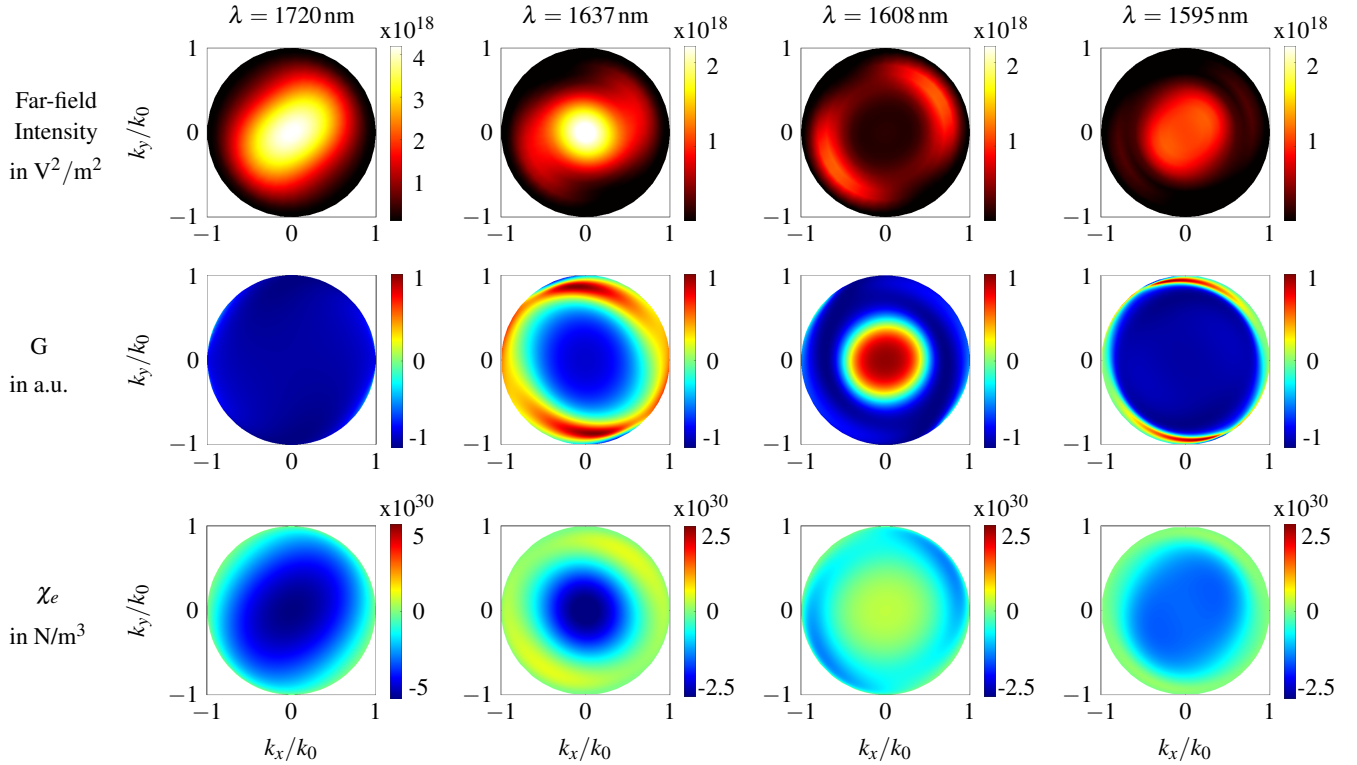
The degree of circular polarization G in the second row of Fig. 3(f) shows that for all pitch numbers the RCP emission angles coincide with the strongest intensities in the far-field. For one and four pitches, this RCP light emission occurs in a broad range of angles centered around the helix axis. For two and three pitches, on the other hand, the RCP emission angles tend to be limited to emission along the antenna axis ($p = 2$) or rotationally symmetric oblique ($p = 3$).

The plots of the electric chirality density χ_e are displayed in the lower row of Fig. 3(f). Both double helices with one and four pitches exhibit a large range of angles for the emission of RCP light, but with a significantly lower intensity for the latter case. While the double helix with three pitches lacks directional emission of RCP light, a very high directivity of RCP emission is obtained for the case of 2 pitches. However, the largest χ_e values are found for the shortest helix, providing nearly perfect directivity and circularly polarized emission while being compact and easy to fabricate.

Conclusion – Plasmonic resonators are an efficient tool to enhance light-matter interaction at the nano-scale and to alter the polarization state of the involved photons. Plasmonic helices, in particular, are able to efficiently couple linearly polarized dipolar emitters to chiral radiation and vice versa. In this numerical study we demonstrated different far-field radiation properties in both directivity and polarization state of helical antennas driven by the same single emitter. For as-



(a)

(b) $\lambda = 1720\text{nm}$ (c) $\lambda = 1637\text{nm}$ (d) $\lambda = 1608\text{nm}$ (e) $\lambda = 1595\text{nm}$ 

(f)

FIG. 3. (a) Purcell enhancement in dependency of the wavelength for a double helix with one, two, three, and four pitches p . The intensity of the electric field strength for pitches p : (b) $p = 1$, (c) $p = 2$, (d) $p = 3$ and (e) $p = 4$. (f) Numerical results for the degree of polarization G , the far-field intensity, and electric chirality density χ_e .

sessing the underlying physics an extended semi-analytical design tool is employed, that evaluates helix geometries for resonance positions and qualitative far-field patterns. Based on this a subsequent full-field modeling proved that a single emitter in a thin film such as hBN can be efficiently coupled to single and double helices. Both antenna geometries provide strong Purcell enhancement in the telecom range, a very small footprint and act as a passive device that does not require electronic control such as phase shifters for polarization control². While the far-field emission angles of the examined single helices show a large variation depending on the mode order, the double helix provides highly directional emission already for a single pitch. The versatility of emission patterns makes the helical antenna a potential building block for different applications such as chiral plasmonic phase gratings³⁸, or sources of circularly polarized single-photons. The latter relies on the high Purcell enhancements in combination with the fact that the emitted photons possess a well-defined spin and a high directivity. In addition, the double helix can act as a device to couple chiral far-fields to the anti-symmetric mode of plasmonic two-wire waveguides³⁹ to realize a highly directional nanoscale polarization converter. Finding optimal helical antenna configurations will speed up in the future by using the semi-analytical model for pre-screening large parameter spaces. Subsequent full field simulations in combination with an optimization algorithm can quantitatively optimize the performance for specific applications. Therewith, we provide a route towards efficient implementation of plasmonic helices in various architectures for photonic quantum technologies.

ACKNOWLEDGMENTS

Funded by the Deutsche Forschungsgemeinschaft (DFG, German Research Foundation) under Germany's Excellence Strategy – The Berlin Mathematics Research Center MATH+ (EXC-2046/1, project ID: 390685689) and also by DFG under project ID HO5461/3-1 "chiralFEBID". This project (20FUN05 SEQUME) has received funding from the EM-PIR programme co-financed by the Participating States and from the European Union's Horizon 2020 research and innovation programme. This project has received funding from the German Federal Ministry of Education and Research (BMBWF Forschungscampus MODAL, project number 05M20ZBM).

DATA AVAILABILITY STATEMENT

The input data files for the FEM simulations, for parameter scans, and the simulation results of this study can be found in a corresponding open access data publication⁴⁰.

¹F. Flamini and N. Spagnolo, "Photonic quantum information processing : a review," *Rep. Prog. Phys.* **82**, 016001 (2019).

²G. Moody, V. J. Sorger, D. J. Blumenthal, P. W. Juodawlkis, W. Loh, C. Sorace-Agaskar, A. E. Jones, K. C. Balram, J. C. F. Matthews, A. Laing, M. Davanco, L. Chang, J. E. Bowers, N. Quack, C. Galland, I. Aharonovich, M. A. Wolff, C. Schuck, N. Sinclair, M. Lončar, T. Komljenovic, D. Weld, S. Mookherjee, S. Buckley, M. Radulaski, S. Reitzenstein, B. Pingault, B. Machielse, D. Mukhopadhyay, A. Akimov,

- A. Zhelitikov, G. S. Agarwal, K. Srinivasan, J. Lu, H. X. Tang, W. Jiang, T. P. McKenna, A. H. Safavi-Naeini, S. Steinhauer, A. W. Elshaari, V. Zwiller, P. S. Davids, N. Martinez, M. Gehl, J. Chiaverini, K. K. Mehta, J. Romero, N. B. Lingaraju, A. M. Weiner, D. Peace, R. Cernansky, M. Lobino, E. Diamanti, L. T. Vidarte, and R. M. Camacho, "2022 Roadmap on integrated quantum photonics," *J. Phys. Photonics* **4**, 12501 (2022).
- ³S. A. Maier, *Plasmonics: Fundamentals and Applications* (Springer, 2007).
- ⁴E. M. Purcell, "Spontaneous Emission Probabilities at Radio Frequencies," *Phys. Rev.* **69**, 681 (1946).
- ⁵K. Kneipp, Y. Wang, H. Kneipp, L. T. Perelman, I. Itzkan, R. R. Dasari, and M. S. Feld, "Single molecule detection using surface-enhanced Raman scattering (SERS)," *Phys. Rev. Lett.* **78**, 1667 (1997).
- ⁶S. Kühn, U. Håkanson, L. Rogobete, and V. Sandoghdar, "Enhancement of single-molecule fluorescence using a gold nanoparticle as an optical nanoantenna," *Phys. Rev. Lett.* **97**, 017402 (2006).
- ⁷A. Kinkhabwala, Z. Yu, S. Fan, Y. Avlasevich, K. Müllen, and W. E. Moerner, "Large single-molecule fluorescence enhancements produced by a bowtie nanoantenna," *Nat. Photonics* **3**, 654 (2009).
- ⁸L. Novotny and N. van Hulst, "Antennas for light," *Nat. Photonics* **5**, 83 (2011).
- ⁹P. Biagioni, J.-S. Huang, and B. Hecht, "Nanoantennas for visible and infrared radiation," *Rep. Prog. Phys.* **75**, 024402 (2012).
- ¹⁰A. F. Koenderink, "Single-photon nanoantennas," *ACS Photonics* **4**, 710 (2017).
- ¹¹T. Feichtner, S. Christiansen, and B. Hecht, "Mode Matching for Optical Antennas," **119**, 217401 (2017).
- ¹²T. H. Taminiau, F. D. Stefani, F. B. Segerink, and N. F. v. Hulst, "Optical antennas direct single-molecule emission," *Nat. Photonics* **2**, 234 (2008).
- ¹³A. G. Curto, G. Volpe, T. H. Taminiau, M. P. Kreuzer, R. Quidant, and N. F. van Hulst, "Unidirectional Emission of a Quantum Dot Coupled to a Nanoantenna," *Science* **329**, 930 (2010).
- ¹⁴J. K. Gansel, M. Thiel, M. S. Rill, M. Decker, K. Bade, V. Saile, G. von Freymann, S. Linden, and M. Wegener, "Gold helix photonic metamaterial as broadband circular polarizer," *Science* **325**, 1513 (2009).
- ¹⁵K. Höflich, T. Feichtner, E. Hansjürgen, C. Haverkamp, H. Kollmann, C. Lienau, and M. Silies, "Resonant behavior of a single plasmonic helix," *Optica* **6**, 1098 (2019).
- ¹⁶I. Fernandez-Corbaton, M. Fruhnert, and C. Rockstuhl, "Objects of maximum electromagnetic chirality," *Phys. Rev. X* **6**, 031013 (2016).
- ¹⁷X. G. Santiago, M. Hammerschmidt, J. Sachs, S. Burger, H. Kwon, M. Knöller, T. Arens, P. Fischer, I. Fernandez-Corbaton, and C. Rockstuhl, "Toward maximally electromagnetically chiral scatterers at optical frequencies," *ACS Photonics* **9**, 1954 (2022).
- ¹⁸M. Wang, R. Salut, H. Lu, M.-A. Suarez, N. Martin, and T. Grosjean, "Sub-wavelength polarization optics via individual and coupled helical traveling-wave nanoantennas," *Light Sci. Appl.* **8**, 76 (2019).
- ¹⁹I. Aharonovich, J.-P. Tetienne, and M. Toth, "Quantum emitters in hexagonal boron nitride," *Nano Lett.* **22**, 9227 (2022).
- ²⁰P. B. Johnson and R.-W. Christy, "Optical constants of the noble metals," *Phys. Rev. B* **6**, 4370 (1972).
- ²¹S.-Y. Lee, T.-Y. Jeong, S. Jung, and K.-J. Yee, "Refractive index dispersion of hexagonal boron nitride in the visible and near-infrared," *Phys. Status Solidi B* **256**, 1800417 (2019).
- ²²"SCHOTT Zemax catalogue 2017-01-20b," (2017).
- ²³J. Pomplun, S. Burger, L. Zschiedrich, and F. Schmidt, "Adaptive finite element method for simulation of optical nano structures," *Phys. Status Solidi B* **244**, 3419 (2007).
- ²⁴L. Zschiedrich, H. J. Greiner, S. Burger, and F. Schmidt, "Numerical analysis of nanostructures for enhanced light extraction from OLEDs," *Proc. SPIE* **8641**, 86410B (2013).
- ²⁵P. Anger, P. Bharadwaj, and L. Novotny, "Enhancement and Quenching of Single-Molecule Fluorescence," *Phys. Rev. Lett.* **96**, 113002 (2006).
- ²⁶F. Marquier, C. Sauvan, and J.-J. Greffet, "Revisiting quantum optics with surface plasmons and plasmonic resonators," *ACS Photonics* **4**, 2091 (2017).
- ²⁷P. Gutsche, L. V. Poulikakos, M. Hammerschmidt, S. Burger, and F. Schmidt, "Time-harmonic optical chirality in inhomogeneous space," *Proc. SPIE* **9756**, 97560X (2016).
- ²⁸L. Novotny, "Effective Wavelength Scaling for Optical Antennas," *Phys. Rev. Lett.* **98**, 266802 (2007).

- ²⁹R. J. Potton, "Reciprocity in optics," *Rep. Prog. Phys.* **67**, 717 (2004).
- ³⁰P. Woźniak, I. De Leon, K. Höflich, C. Haverkamp, S. Christiansen, G. Leuchs, and P. Banzer, "Chiroptical response of a single plasmonic nanohelix," *Opt. Express* **26**, 1513 (2018).
- ³¹J. Petschulat, D. Cialla, N. Janunts, C. Rockstuhl, U. Hübner, R. Möller, H. Schneidewind, R. Mattheis, J. Popp, A. Tünnermann, F. Lederer, and T. Pertsch, "Doubly resonant optical nanoantenna arrays for polarization resolved measurements of surface-enhanced Raman scattering," *Opt. Express* **18**, 4184 (2010).
- ³²V. G. Kravets, A. V. Kabashin, W. L. Barnes, and A. N. Grigorenko, "Plasmonic Surface Lattice Resonances: A Review of Properties and Applications," *Chem. Rev.* **118**, 5912 (2018).
- ³³V. V. Klimov, M. Ducloy, and V. S. Letokhov, "Spontaneous emission of an atom in the presence of nanobodies," *Quantum Electron.* **31**, 569 (2001).
- ³⁴E. R. Encina, E. M. Perassi, and E. A. Coronado, "Near-Field Enhancement of Multipole Plasmon Resonances in Ag and Au Nanowires," *J. Phys. Chem. A* **113**, 4489 (2009).
- ³⁵A. L. Exarhos, D. A. Hopper, R. R. Grote, A. Alkauskas, and L. C. Bassett, "Optical Signatures of Quantum Emitters in Suspended Hexagonal Boron Nitride," *ACS Nano* **11**, 3328 (2017).
- ³⁶H. Takashima, H. Maruya, K. Ishihara, T. Tashima, K. Shimazaki, A. W. Schell, T. T. Tran, I. Aharonovich, and S. Takeuchi, "Determination of the Dipole Orientation of Single Defects in Hexagonal Boron Nitride," *ACS Photonics* **7**, 2056 (2020).
- ³⁷A. Moradi, "Plasmon hybridization in parallel nano-wire systems," *Phys. Plasmas* **18**, 064508 (2011).
- ³⁸J. Lin, J. P. B. Mueller, Q. Wang, G. Yuan, N. Antoniou, X.-C. Yuan, and F. Capasso, "Polarization-controlled tunable directional coupling of surface plasmon polaritons," *Science* **340**, 331 (2013).
- ³⁹J.-S. Huang, T. Feichtner, P. Biagioni, and B. Hecht, "Impedance Matching and Emission Properties of Nanoantennas in an Optical Nanocircuit," *Nano Lett.* **9**, 1897 (2009).
- ⁴⁰L. Kuen, L. Löffler, A. Tsarapkin, L. Zschiedrich, T. Feichtner, S. Burger, and K. Höflich, "Source code and simulation results: Chiral and directional optical emission from a dipole source coupled to a helical plasmonic antenna," Zenodo, DOI: 10.5281/zenodo.10598256 (2024).